Available online at www.sciencedirect.com

ScienceDirect

Energy Procedia 126 (201709) 706–713

Energy Procedia

www.elsevier.com/locate/procedia

72nd Conference of the Italian Thermal Machines Engineering Association, ATI2017, 6–8 September 2017, Lecce, Italy

On the Hysteretic Behaviour of Wells Turbines

Tiziano Ghisu[a,*], Pierpaolo Puddu[a], Francesco Cambuli[a], Irene Virdis[a]

[a]Dipartimento di Ingegneria Meccanica, Chimica e dei Materiali, Università degli Studi di Cagliari, via Marengo 2, 09123 Cagliari, Italy

Abstract

The Wells turbine is a self-rectifying axial flow turbine employed in Oscillating Water Column systems to convert low-pressure airflow into mechanical energy. A number of studies highlighted a variation in turbine performance between acceleration and deceleration phases, generally ascribed to the interaction between blade trailing edge vortices and blade boundary layer. This explaination is in opposition with the large existing literature on rapidly pitching airfoils and wings, where it is generally accepted that a hysteretic behavior can be appreciated only at non-dimensional frequencies significantly larger than the ones typically found in Wells turbine.

This work presents a critical re-examination of the phenomenon and a new analysis of some of the test cases originally used to explain its origin. The results demonstrate how the behavior of a Wells turbine is not dissimilar to that of an airfoil pitching at very low reduced frequencies and that the causes of the alleged hysteresis are in a different phenomenon.

Peer-review under responsibility of the scientific committee of the 72nd Conference of the Italian Thermal Machines Engineering Association

Nomenclature

μ	fluid viscosity	r	radius
ω	angular velocity	r^*	non-dimensional radius $(r-r_h)/(r_{tip}-r_h)$
Ω_t	tangential component of vorticity	r_h	hub radius
ϕ	global flow coefficient	r_{tip}	tip radius
ϕ_l	local flow coefficient	T	torque
ρ	density	T^*	non-dimensional torque
σ	solidity at tip radius	T^{**}	local non-dimensional torque
τ_w	wall shear stress	V_a	absolute axial velocity
c	blade chord	V_t	absolute tangential velocity
c_p	pressure coefficient	W	relative velocity magnitude
f	piston frequency	W_a	relative axial velocity
$\bar{f}$	non-dimensional piston frequency	W_t	relative tangential velocity
P	static pressure	x	blade coordinate in the direction of the chord
P^*	non-dimensional static pressure drop	y	wall distance
P^{**}	local non-dimensional static pressure drop	y^+	non-dimensional wall distance $(y\sqrt{\rho\tau_w}/\mu)$

*Corresponding author. E-mail: t.ghisu@unica.it

1876-6102
Peer-review under responsibility of the scientific committee of the 72nd Conference of the Italian Thermal Machines Engineering Association
10.1016/j.egypro.2017.08.303

1. Introduction

The Wells turbine [1] is a self-rectifying axial flow turbine employed, with a Oscillating Water Column (OWC) system, to convert sea wave energy in mechanical energy [2]. Its performance has been studied extensively, both experimentally [3, 4, 5, 6, 7, 8] and numerically [9, 10, 11, 12, 13, 14]. One peculiar aspect mentioned in this research is the apparent difference in performance during the accelerating and decelerating phases of the normal operation. The first investigation of this phenomenon was presented by Setoguchi *et al.* [5]. Their facility employed a large cylinder with a moving piston connected to the turbine duct, so as to reproduce the OWC system dynamics and a realistic bi-directional airflow. Different rotor geometries were studied, highlighting the lower performance of the machine during piston acceleration than during deceleration (counter-clockwise hysteretic loop). The hysteresis was present even with a maximum angle of attack significantly lower than the one corresponding to static stall.

They concluded the phenomenon (a) unlikely to be caused by three-dimensional effects, because of the independency from blade aspect ratio, and (b) to be dissimilar to the one present in airfoils and wings, because of the opposite rotation of the hysteresis cycle. However, they did not mention that counter-clockwise loops do develop in airfoils at lower-incidence-angle excursions, with the flow still attached to the surface [15], while clockwise hysteretic loops are present in pitching wings only at large angles of attack (when vortex burst or stall are enclosed in the pitch excursion).

Setoguchi *et al.* [16] and Kinoue *et al.* [10, 17] employed Computational Fluid Dynamics (CFD) to explain the origin of the phenomenon, studying a simplified geometry (a blade passage of the straight annular duct housing the turbine rotor, neglecting the piston chamber). They identified different vortical structures during acceleration and deceleration, and attributed the different performance to their interaction with trailing edge vortices shed by the blade.

In this work, the Wells turbine of Setoguchi *et al.* [5] is studied numerically, initially with the geometrical simplification of [16, 10, 17] and then with a geometry more representative of the experimental setup. This allows the performance of the turbine to be isolated from that of the OWC system and verify whether the difference in performance highlighted in the experiments is caused by a real hysteresis of the turbine, or by some other phenomenon.

2. Methodology

The experimental set-up and the details of the investigation are reported in [5]. The experimental facility is composed of a cylindrical chamber (1.4 m diameter) with a piston moved by an electric motor. The airflow is conveyed in an annular duct where the Wells turbine is placed. Main geometric and flow characteristics are reported in Table 1. During the experiment, the turbine operated at Reynolds numbers between 1.3×10^5 and 3.1×10^5 ($Re = \frac{\rho W c}{\mu}$), while the reduced frequency ($\overline{f} = (\pi f c)/(\omega r_{tip})$) ranged between 8×10^{-4} and 1.4×10^{-3}. In this work, the analysis focuses on the NACA0020 turbine, with 1 mm tip clearance and 90 mm chord length (solidity at tip radius $\sigma = 0.67$).

Table 1. Wells turbine geometry analyzed in [5]

Airfoil	NACA 0015/0018/0020	Rotor Tip Diameter	300 mm
Rotor hub diameter	110 mm	Tip clearance	1/2/3 mm
Chord length	60/90/108 mm	Number of blades	5/6/7
Solidity at tip radius	0.48-0.67	Sweep ratio	0.420 (37.5/90)
Rotational speed	2500 rpm	Piston period	6 s

Setoguchi *et al.* [16] and Kinoue *et al.* [10, 17] conducted a numerical study on a simplified geometry (a straight annular duct enclosing the turbine rotor, as in Figure 1, top left) to simulate the performance of the machine. This geometry has been used in this work to verify the hysteresis reported by [16, 10, 17]. Then, a more realistic geometry (including moving piston, chamber and actual duct) has been employed to verify the effects of the previous simplification both on flow distribution and on the hysteretic characteristics of the machine.

The numerical simulations have been conducted with the commercial CFD software Ansys Fluent® 15.0, while Ansys IcemCFD® has been used to generate the multi-block structured grid (Figure 1). A C-grid around the blade was able to capture the complex boundary layer flow, with a H-mesh structure in the rest of domain. The unsteady Reynolds-Averaged Navier-Stokes (RANS) equations have been solved for a compressible ideal gas. Based on the

results of Ghisu *et al.* [18, 19], the $k-\omega$ SST model has been selected for turbulence closure. The SIMPLEC algorithm has been used for pressure-velocity coupling, a second-order upwind scheme for discretizing convective terms and a second-order centered scheme for pressure and viscous terms.

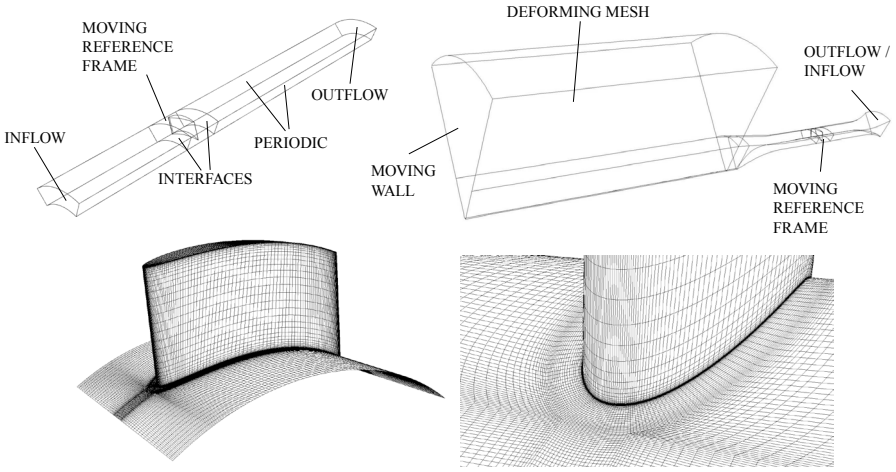

Fig. 1. Simplified (top left) and full (top right) computational domains, and computational mesh (bottom)

The motion of the piston has been simulated by means of a moving wall, controlled by an user-defined-function (UDF), in combination with a dynamic mesh. One passage has been simulated, with periodic boundary conditions. The interaction between stationary and rotating frames has been simulated using a frozen rotor approach [20].

A grid sensitivity study similar to the one of [21] has been conducted to verify the choice of the numerical mesh. As a result, a mesh with 260 points around the blade profile, 70 between successive blades (in the wake region) and 35 in spanwise direction was obtained. 10 points have been employed in the tip gap region, for a total of about 10^6 cells, and the maximum non-dimensional wall distance y^+ was of the order of 1.

3. Results

3.1. A Comparison with Unsteady Forces in Rapidly Pitching Airfoils

A Wells turbine blade, during its normal operation, experiences a periodic change in incidence angle, due to the bi-directional airflow generated by the motion of the (water) piston inside the OWC. This is not dissimilar to what happens to rapidly pitching (or plunging) airfoils, where the presence of a hysteretic loop for the force coefficients has been known for many decades and analyzed with great level of details since the 1970s [22, 23], for its importance in various applications. The phenomenon is dominated by two parameters: maximum incidence angle and reduced frequency, while the importance of Reynolds number is limited. The maximum incidence angle defines whether and to what extent the airfoil experiences stall, while the reduced frequency determines the importance of dynamic effects, generating a difference between force coefficients during pitch-up and pitch-down. Figure 2 presents a comparison between the experimental data of McCroskey [23] and computational results obtained in this work using unsteady RANS ($k-\omega$ turbulence model). The NACA0012 airfoil is sinusoidally pitching with an incidence range of 20 degrees around different mean angles, at a fixed reduced frequency of 0.1, in different stall conditions. In no-stall conditions (i.e. maximum incidence angle lower than static stall angle) the motion determines a counter-clockwise hysteretic loop, while in deep-stall conditions the loop is clockwise. In intermediate situations, the loop is distorted, and in some cases (light-stall) a bow appears in the lift coefficient loop. These dynamic effects have been know for decades and studied in detail both experimentally [22, 23] and numerically [15]. They are generally considered negligible at reduced frequencies lower that $4 \cdot 10^{-3}$ [22]. The reduced frequencies Wells turbines operate at are not sufficient to produce hysteretic effects in isolated airfoils and wings.

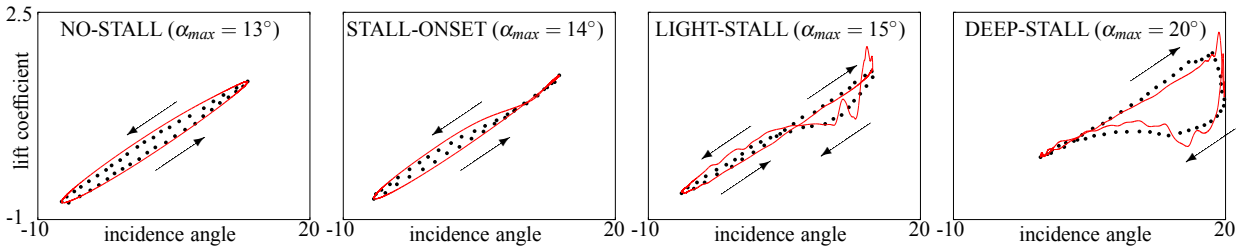

Fig. 2. Numerical results (red curve) for the lift coefficient in rapidly pitching airfoils, for different stall conditions, and comparison with experiments (circles) [23]

3.2. Simplified Geometry

Wells turbine performance is reported in terms of non-dimensional pressure drop and torque as a function of the flow coefficient ϕ. ΔP is the pressure difference across the rotor, ρ is the flow density, ω the angular velocity, r_{tip} the tip radius, T the torque and V_a the axial velocity upstream of the rotor. In the experimental analysis of Setoguchi *et al.* [5], V_a is not directly measured, but its value is calculated from piston velocity and area ratio (ratio between piston area and rotor inlet area), considering capacitive effects negligible, while a similar assumption needs to be always carefully verified when dealing with dynamic systems [7]. This makes ϕ a theoretical flow coefficient:

$$T^* = \frac{T}{\rho\omega^2 r_{tip}^5}; \quad P^* = \frac{\Delta P}{\rho\omega^2 r_{tip}^2}; \quad \phi = \frac{V_a}{\omega r_{tip}} \equiv \frac{V_{piston}}{\omega r_{tip}} \frac{A_{piston}}{A_{rotor}} \tag{1}$$

Following the approach of [16, 10, 17], V_a is imposed as an inlet boundary condition, together with turbulence intensity (3%) and viscosity ratio (10). These values are representative of a quiet flow. Torresi *et al.* [12] verified the neglible influence of turbulence parameters on Wells turbine performance. Ambient static pressure is imposed at exit.

A transient simulation has been run, with a first-order implicit approach in time and different values for the time step, keeping the number of sub-iterations fixed and equal to 20. The inlet velocity has been varied using a sinusoidal law, to obtain the same flow coefficient that would have been caused by the motion of the piston and assuming capacitive effects in the OWC system negligible. The simulations, initialized with the steady solution at $\phi = 0$, have been run for half a period (corresponding to the outflow phase). Figure 3 highlights the importance of a correct choice of the time-step in transient simulations: when selected appropriately, these simulations do not show any hysteresis between acceleration and deceleration phases, and no difference between the steady and transient performance.

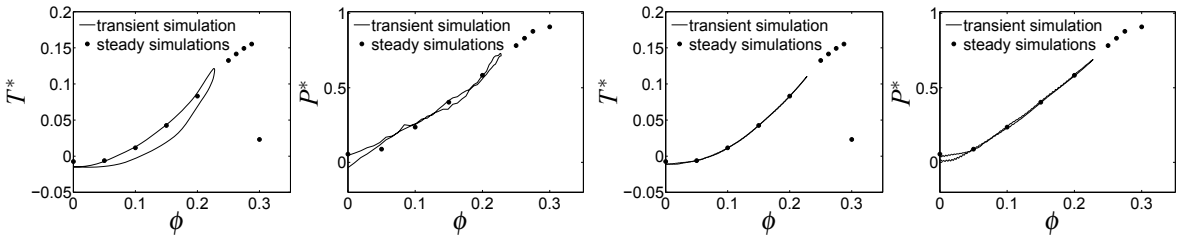

(a) $\Delta t = 2 \cdot 10^{-2} s$ (b) $\Delta t = 1.25 \cdot 10^{-3} s$

Fig. 3. Influence of time-step size in transient simulations

3.3. Full Geometry

The simulations with the full geometry (Figure 1, top right) have been run for three piston periods to verify that periodically stable results had been obtained. A time step of $5 \cdot 10^{-4}$ s has been used. Figure 4 compares the non-dimensional coefficients of torque and static pressure drop with the experimental data of [5].

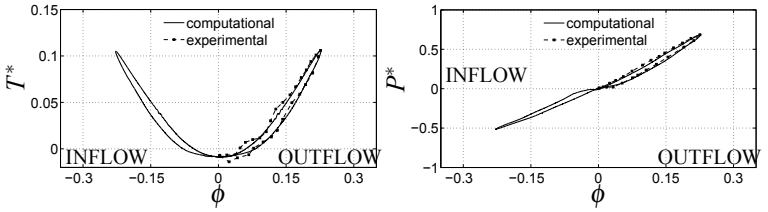

Fig. 4. Comparison between experimental and computational results

The flow coefficient ϕ is calculated from piston velocity and system geometry (equation (1)), assuming the flow at inlet to the turbine to be axial and assuming capacitive effects negligible (as in [5]). The experimental data are available only during outflow, while numerical results are available both for inflow (negative flow coefficient) and outflow (positive flow coefficient). The hysteresis of the real OWC system is evident and is correctly reproduced.

To isolate the turbine aerodynamic behavior, performance should be correlated to flow characteristics near the blade. Torque and pressure drop have been non-dimensionalized as in equations (2), with local values of (tangentially-averaged) relative velocity evaluated $0.5c$ upstream of the rotor, rather than with blade tip speed as in equations (1), and plotted as a function of a local flow coefficient ϕ_l, calculated at mid-radius. This non-dimensionalization allows the evaluation of effective force coefficients on the blade, as in common practices for wings [23] and turbomachinery. The results (Figure 5), do not show significant differences between performance during acceleration and deceleration.

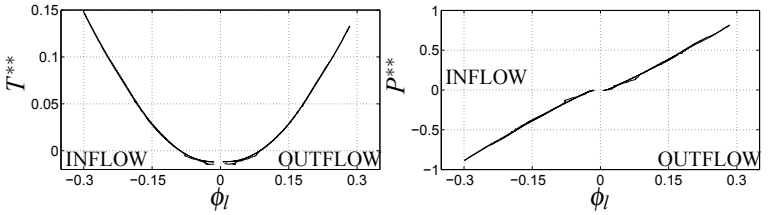

Fig. 5. Computational performance as a function of local flow variables

$$T^{**} = \frac{T}{\rho W_t^2 r_{tip}^3}; \quad P^{**} = \frac{\Delta P}{\rho W_t^2}; \quad \phi_l = \frac{W_a}{W_t}; \tag{2}$$

It is important to verify the flow behavior near the rotor and the presence of the vortical structures shown by [16, 10, 17]. Figure 6(a) shows the difference in radial distributions of axial velocity upstream of the rotor between acceleration and deceleration, during outflow, for two values of (global) flow coefficient based on piston velocity. The differences are caused by capacitive effects due to the chamber volume and are the real cause of the hysteresis. Figure 6(b) compares the axial velocity distributions for equal mass-flows through the rotor during acceleration and deceleration.

Figure 7 shows a comparison of pressure coefficient distributions at mid-span: at equal values of global flow coefficient ϕ, the different axial velocity determines a different pressure coefficient distribution and therefore the apparent hysteresis seen in Figure 4. When the local flow coefficents (ϕ_l) is the same, the mass-flow through the rotor is equal and the difference in pressure distribution between acceleration and deceleration vanishes.

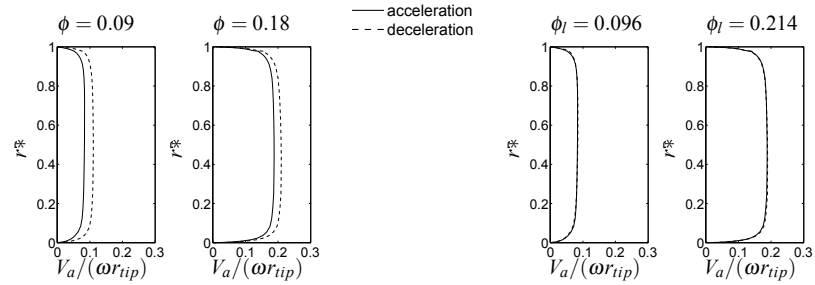

(a) Equal global flow coefficients (ϕ) (b) Equal local flow coefficients (ϕ_l)

Fig. 6. Spanwise distribution of axial velocity during acceleration and deceleration

Figure 8 compares relative velocity contours around the blade for the two values of the local flow coefficient ϕ_l. The differences are minimal, and not sufficient to produce appreciable variations in the pressure coefficient distributions or in the values of the integral forces. The flow is well attached to the turbine blade over most of the span, with the appearance of a confined corner separation near the hub. The large areas of flow separation presented in the numerical work of Setoguchi *et al.* and Kinoue *et al.* [5, 10, 17] have not been found in this work.

Figures 10 and 11 highlight the main secondary flow structures present in the flow during acceleration and deceleration, at $\phi_l = 0.096$ and $\phi_l = 0.214$, respectively. Tip leakage vortex and horseshoe vortices near the hub at either sides of the blade are evident for both flow coefficients, and their intensity increases at $\phi_l = 0.214$.

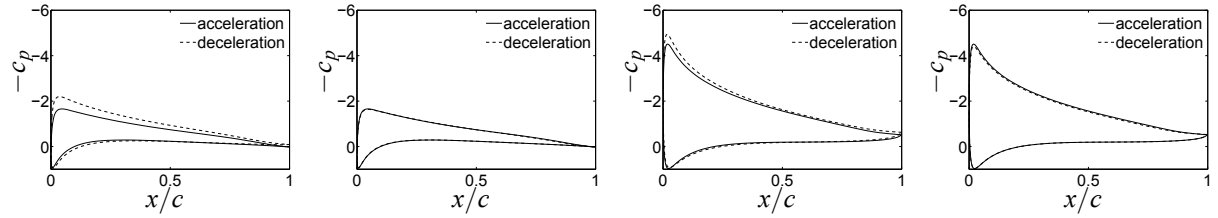

(a) $\phi = 0.09$ (b) $\phi_l = 0.096$ (c) $\phi = 0.18$ (d) $\phi_l = 0.214$

Fig. 7. Mid-span pressure coefficient distributions during acceleration and deceleration, for the same values of global and local flow coefficient

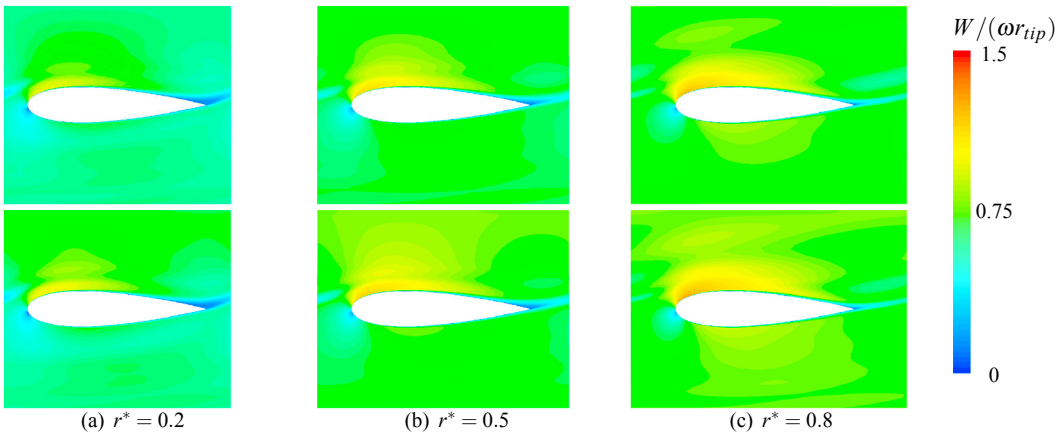

(a) $r^* = 0.2$ (b) $r^* = 0.5$ (c) $r^* = 0.8$

Fig. 8. Comparison of relative velocity contours during acceleration (top) and deceleration (bottom), at different radial positions (r^*), for $\phi_l = 0.096$

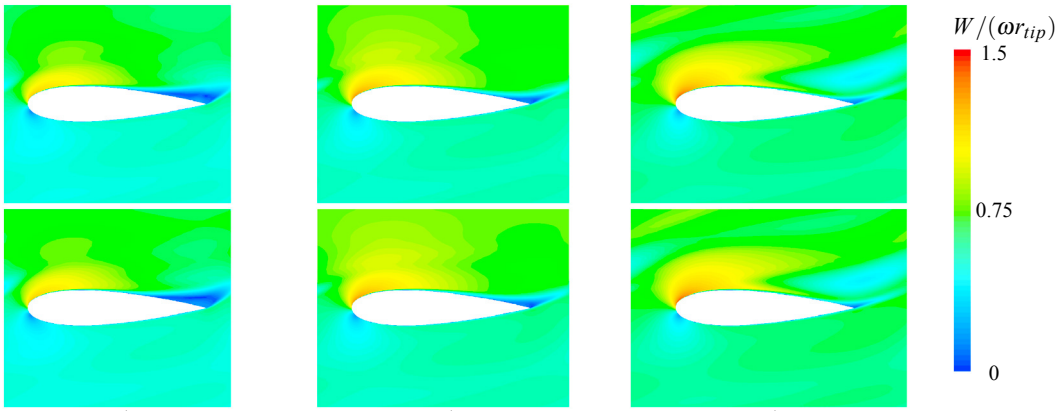

Fig. 9. Comparison of relative velocity contours during acceleration (top) and deceleration (bottom), at different radial positions (r^*), for $\phi_l = 0.214$

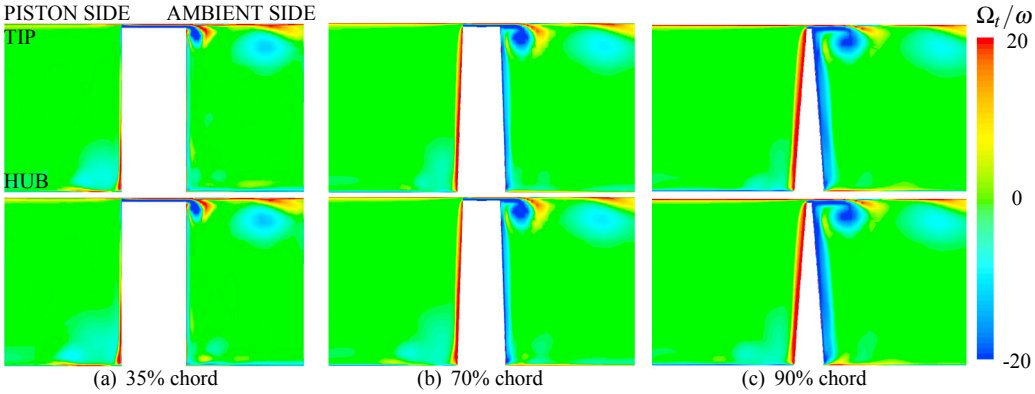

Fig. 10. Tangential vorticity contours at $\phi_l = 0.096$ during acceleration (top) and deceleration (bottom), at planes with different tangential positions.

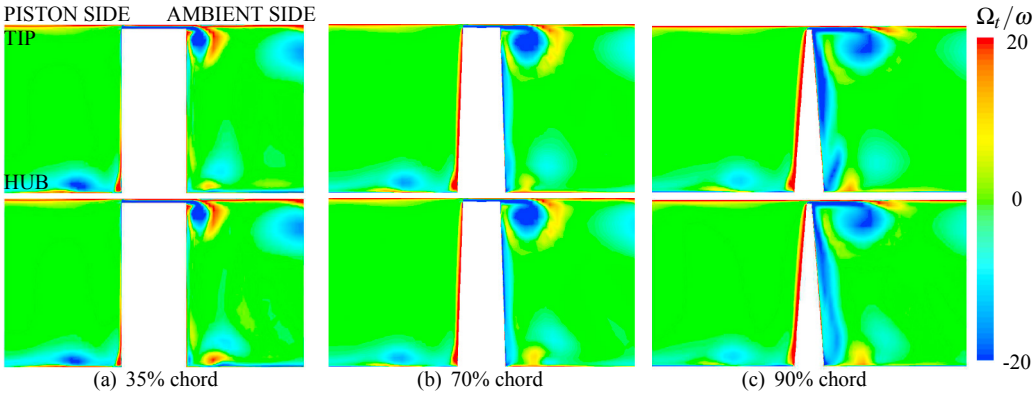

Fig. 11. Tangential vorticity contours at $\phi_l = 0.214$ during acceleration (top) and deceleration (bottom), at planes with different tangential positions.

The strength of the horseshoe vortices decreases significantly towards the trailing edge, and vortices produced by previous blades are barely visible, while the larger intensity of the tip leakage vortex makes it visible also near the following blade. The differences between acceleration and deceleration are minimal and confined to small regions, and do not produce appreciable variations in the integral forces produced by the blade.

4. Conclusion

The existence of a hysteretic behavior in Wells turbines has been recognized by several authors. Nevertheless, operating non-dimensional frequencies are significantly lower than the ones studied for pitching airfoils and wings, where the phenomenon has been investigated extensively. [16, 10, 17] used Computational Fluid Dynamics to analyze the problem and found its origin in the interaction between secondary flow structures and trailing edge vortices.

A numerical analysis of the same problem is presented, first using the simplifications of [16, 10, 17], then with a geometry more representative of the actual experimental setup. The behavior of the turbine has been isolated from the one of the OWC system. The origin of the hysteresis has been demonstrated to be linked to capacitive effects within the OWC system rather than to dynamic effects in the turbine. These effects are negligible, at least at the non-dimensional frequencies and Reynolds number studied in this problem. The phenomena indicated by other authors as the causes for the hysteretic behavior have not been confirmed in this analysis.

References

[1] A. Wells, Fluid Driven Rotary Transducer - BR. Pat. 1595700 (1976).
[2] A. F. de O. Falcao, Wave energy utilization: A review of the technologies, Renewable and Sustainable Energy Reviews 14 (3) (2010) 899–918.
[3] L. M. C. Gato, A. F. de O. Falcao, Aerodynamics of the wells turbine, International Journal of Mechanical Sciences 30 (6) (1988) 383–395.
[4] R. Curran, L. M. C. Gato, The energy conversion performance of several types of Wells turbine designs, Proceedings of the Institution of Mechanical Engineers, Part A: Journal of Power and Energy 211 (2) (1997) 133–145.
[5] T. Setoguchi, M. Takao, K. Kaneko, Hysteresis on wells turbine characteristics in reciprocating flow, International Journal of Rotating Machinery 4 (1) (1998) 17–24.
[6] A. Thakker, R. Abdulhadi, Effect of Blade Profile on the Performance of Wells Turbine under Unidirectional Sinusoidal and Real Sea Flow Conditions, International Journal of Rotating Machinery 2007 (2007) 1–9. doi:10.1155/2007/51598.
[7] M. Paderi, P. Puddu, Experimental investigation in a Wells turbine under bi-directional flow, Renewable Energy 57 (2013) 570–576. doi:10.1016/j.renene.2013.02.016.
[8] P. Puddu, M. Paderi, C. Manca, Aerodynamic Characterization of a Wells Turbine under Bi-directional Airflow, Energy Procedia 45 (2014) 278–287. doi:10.1016/j.egypro.2014.01.030.
[9] T. Kim, T. Setoguchi, Y. Kinoue, K. Kaneko, Effects of blade geometry on performance of wells turbine for wave power conversion, Journal of Thermal Science 10 (4) (2001) 293–300. doi:10.1007/s11630-001-0035-4.
[10] Y. Kinoue, T. Setoguchi, T. H. Kim, K. Kaneko, M. Inoue, Mechanism of Hysteretic Characteristics of Wells Turbine for Wave Power Conversion, Journal of Fluids Engineering 125 (2) (2003) 302–307. doi:10.1115/1.1538629.
[11] T. S. Dhanasekaran, M. Govardhan, Computational analysis of performance and flow investigation on wells turbine for wave energy conversion, Renewable Energy 30 (14) (2005) 2129–2147. doi:10.1016/j.renene.2005.02.005.
[12] M. Torresi, S. M. Camporeale, G. Pascazio, Detailed CFD Analysis of the Steady Flow in a Wells Turbine Under Incipient and Deep Stall Conditions, Journal of Fluids Engineering 131 (7) (2009) 071103–1–071103–17. doi:10.1115/1.3155921.
[13] R. Gomes, J. Henriques, L. Gato, A. FalcÃčo, Hydrodynamic optimization of an axisymmetric floating oscillating water column for wave energy conversion, Renewable Energy 44 (2012) 328–339. doi:10.1016/j.renene.2012.01.105.
[14] R. Soltanmohamadi, E. Lakzian, Improved Design of Wells Turbine for Wave Energy Conversion Using Entropy Generation, Meccanica (2015) 1–10doi:10.1007/s11012-015-0330-x.
[15] G. N. Barakos, D. Drikakis, Computational study of unsteady turbulent flows around oscillating and ramping aerofoils, International Journal for Numerical Methods in Fluids 186 (2003) 163–186.
[16] T. Setoguchi, Y. Kinoue, T. H. Kim, K. Kaneko, M. Inoue, Hysteretic characteristics of Wells turbine for wave power conversion, Renewable Energy 28 (13) (2003) 2113–2127.
[17] Y. Kinoue, T. H. Kim, T. Setoguchi, M. Mohammad, K. Kaneko, M. Inoue, Hysteretic characteristics of monoplane and biplane Wells turbine for wave power conversion, Energy Conversion and Management 45 (9-10) (2004) 1617–1629.
[18] T. Ghisu, P. Puddu, F. Cambuli, Numerical Analysis of a Wells Turbine at Different Non-dimensional Piston Frequencies, Journal of Thermal Science 24 (6) (2015) 535–543. doi:10.1007/s11630-015-0819-6.
[19] T. Ghisu, P. Puddu, F. Cambuli, A Detailed Analysis of the Unsteady Flow within a Wells Turbine, Proceedings of the Institution of Mechanical Engineers Part A Journal of Power and Energy 231 (3) (2017) 197–214.
[20] Ansys Fluent User's Guide. Software release 15.0.
[21] T. Ghisu, P. Puddu, F. Cambuli, Physical Explanation of the Hysteresis in Wells Turbines: a Critical Reconsideration, ASME Journal of Fluids Engineering 133 (11). doi:10.1115/1.4033320.
[22] L. W. Carr, K. W. McAlister, W. J. McCroskey, Analysis of the development of dynamic stall based on oscillating airfoil experiments, Tech. Rep. January (1977).
[23] W. J. McCroskey, The Phenomenon of Dynamic Stall, Tech. rep. (1981). doi:10.1080/6008555886.